

# Optically Detected Magnetic Resonance of Nitrogen-Vacancy Centers in Diamond under Weak Laser Excitation

Yong-Hong Yu,<sup>1,2</sup> Rui-Zhi Zhang,<sup>1,2</sup> Yue Xu,<sup>1,2</sup> Xiu-Qi Chen,<sup>1,2</sup> Huijie Zheng,<sup>1,3,\*</sup> Quan Li,<sup>4</sup> Ren-Bao Liu,<sup>4</sup> Xin-Yu Pan,<sup>1,3,5</sup> Dmitry Budker,<sup>6,7,8</sup> and Gang-Qin Liu<sup>1,3,5,†</sup>

<sup>1</sup>*Beijing National Laboratory for Condensed Matter Physics,*

*Institute of Physics, Chinese Academy of Sciences, Beijing 100190, China*

<sup>2</sup>*School of Physical Sciences, University of Chinese Academy of Sciences, Beijing 100049, China*

<sup>3</sup>*Songshan Lake Materials Laboratory, Dongguan, Guangdong 523808, China*

<sup>4</sup>*Department of Physics, Centre for Quantum Coherence,*

*and The Hong Kong Institute of Quantum Information Science and Technology,*

*The Chinese University of Hong Kong, New Territories, Hong Kong, China*

<sup>5</sup>*CAS Center of Excellence in Topological Quantum Computation, Beijing 100190, China*

<sup>6</sup>*Johannes Gutenberg-Universität Mainz, 55128 Mainz, Germany*

<sup>7</sup>*Helmholtz-Institut, GSI Helmholtzzentrum für Schwerionenforschung, 55128 Mainz, Germany*

<sup>8</sup>*Department of Physics, University of California, Berkeley, California 94720, USA*

(Dated: August 28, 2023)

As promising quantum sensors, nitrogen-vacancy (NV) centers in diamond have been widely used in frontier studies in condensed matter physics, material sciences, and life sciences. In practical applications, weak laser excitation is favorable as it reduces the side effects of laser irradiation, for example, phototoxicity and heating. Here we report a combined theoretical and experimental study of optically detected magnetic resonance (ODMR) of NV-center ensembles under weak 532-nm laser excitation. In this regime, both the width and splitting of ODMR spectra decrease with increasing laser power. This power dependence is reproduced with a model considering laser-induced charge neutralization of  $\text{NV}^-$ - $\text{N}^+$  pairs in the diamond lattice. These results are important for understanding and designing NV-based quantum sensing in light-sensitive applications.

Spin defects in solid with optical interface are among the leading platforms for quantum information science and quantum sensing. Among the many spin defects, the negatively charged nitrogen-vacancy ( $\text{NV}^-$ ) center in diamond stands out as having superb spin coherence, bright photoluminescence, and large contrast of magnetic resonance signal [1]. For quantum sensing applications, these features bring remarkable sensitivity in detecting magnetic field [2–4], temperature [5, 6], pressure and other physical quantities [7, 8]. Meanwhile, the atomic structure of an NV center enables spatial resolution down to the nanoscale, and the ultra-stable diamond structure is compatible with complex biochemical environments [9], even in extreme conditions including megabar pressures [10] or sub-kelvin temperatures [11].

Laser excitation provides an efficient and convenient route to establishing the polarization and readout of NV electron spin, and it has been widely used in NV-based quantum techniques. In practical applications, however, laser excitation also brings unwanted side effects. For example, phototoxicity is an important issue in living cell studies using fluorescent probes, and recent experiments have shown that even weak laser excitation could bring adverse effects to living cells [12, 13]. Another side effect is light-induced sample heating, which becomes a serious impediment to temperature-sensitive applications, such as characterizing superconducting films or magnetic

films with low transition temperatures [11, 14–17], and temperature-cell division during early embryogenesis [18].

A straightforward strategy to reduce the laser-induced side effects is using laser beams of sufficiently low intensity, but the intrinsic properties of NV centers, including charge, spin, and optical properties, have been insufficiently studied under weak excitation. Jensen *et al* reported light-narrowing of microwave power-broadened magnetic resonance signals of NV centers under a small magnetic field, which was ascribed to the light-induced decrease of NV spin relaxation time ( $T_1$ ) [19]. Under optical pumping, the charge conversion of an NV center (between  $\text{NV}^-$  and  $\text{NV}^0$ ) is inevitable [20], and the randomly distributed charges, either from NV centers or from nearby charge traps, creating internal electric fields around the NV center [21]. It is thus necessary to take into account both the charge and spin degrees of freedom together and reconsider the magnetic resonance of NV centers under weak laser excitation. Recently, Manson *et al* made an important step in this direction, demonstrating that charge conversation of  $\text{NV}^-$ - $\text{N}^+$  pairs is critical for understanding the optical properties of the NV centers in diamond [22].

In this letter, we report a combined theoretical and experimental study on optically detected magnetic resonance (ODMR) of NV centers under weak green laser (532 nm) excitation. Ensembles of NV centers in nanodiamonds, microdiamonds, and bulk diamonds are studied. When the excitation laser power is much (one or more order of magnitude) smaller than the optical saturation power, both the width and splitting of ODMR

\* hjzheng@iphy.ac.cn

† gqliu@iphy.ac.cn

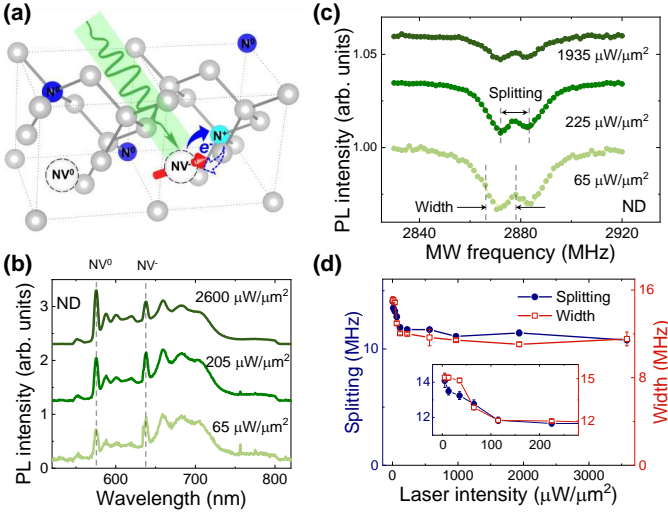


FIG. 1. Laser-induced charge neutralization of  $NV^- N^+$  pairs in diamond. (a) Schematic of the  $NV^- N^+$  model. After absorbing photons,  $NV^- N^+$  pairs could change into  $NV^0 N^0$  pairs, resulting in a more dilute charge distribution in the diamond lattice and thus smaller internal electric fields acting on the remaining NV centers. (b) Photoluminescence (PL) spectra of a nanodiamond measured at 8.4 K. The curves are vertically offset for clarity. Notice the relative changing of the  $NV^-/NV^0$  zero-phonon lines as a function of the laser intensity. (c) Optically detected magnetic resonance (ODMR) spectra of the same nanodiamond measured under different laser powers. (d) Laser power dependence of the ODMR splitting and width. Inset: zoom-in of the weak excitation region.

spectra decrease with increasing laser power. This unexpected phenomenon is well interpreted with a model considering laser-induced charge neutralization of  $NV^- N^+$  pairs in diamond.

*(Results)* A nitrogen-vacancy center is formed by a substitutional nitrogen atom and a nearby vacancy in the diamond lattice. It has two common charge states,  $NV^-$  and  $NV^0$ , with featured zero-phonon lines (ZPL) at 637 nm and 574 nm, respectively. The negatively charged  $NV^-$  center is a natural spin qubit, it presents spin-dependent optical transitions, which enable high-fidelity spin polarization and readout through optical methods. By contrast, it is more challenging to initialize and read out the spin state of an  $NV^0$  center (a spin-half system) [23]. Laser excitation induces charge conversions of NV centers (between  $NV^-$  and  $NV^0$ ), either through a two-photon or single-photon ionization processes [20, 24].

The key finding of this work is that the internal electric field around an NV center is mainly determined by its nearby substitutional nitrogen atoms and can be modified by the excitation light, with the effect becoming more prominent in the weak excitation regime. It is generally believed that the extra electron of an  $NV^-$  is captured from a nearby defect, for example, another nitrogen atom (P1 center) [22]. In this scenario, the negatively charged  $NV^-$  center is often accompanied by a positively charged

$N^+$ . Although the diamond is electrically neutral overall, these randomly distributed charges ( $NV^-$ ,  $N^+$ , and other charge traps) bring about internal electric fields at the NV positions [21]. Under laser excitation, the charge distribution and related internal electric field in the diamond lattice are modified, which brings observable changes to the optical and spin properties of the remaining NV centers, as illustrated in Fig. 1a.

We start by measuring the photoluminescence (PL) spectra of NV centers under weak laser excitation. Nanodiamonds (NDs) with ensemble NV centers are deposited on strontium titanate (or alumina) substrates and measured in a home-built confocal microscopy. The average size of NDs is about 100 nm, with NV concentration of about 3 ppm (Adamas). Figure 1b shows the typical PL spectra of these NDs, measured at 8.4 K. The ZPL of  $NV^-$  (637 nm) and  $NV^0$  (574 nm) are well resolved. The relative amplitude of the two peaks shows pronounced laser power dependence. In the weak excitation region, that is, when the excitation laser is about two-orders of magnitude weaker than the saturation power (see Fig. S1 for laser-power dependence of NV counts), ZPL of  $NV^-$  is stronger than that of  $NV^0$ . In the strong excitation region, on the contrary, ZPL of  $NV^0$  becomes stronger. We note similar phenomenon has been observed recently [25].

Next, we show that the laser-induced charge conversion also strongly affects the NV magnetic resonance signal. ODMR spectra of  $NV^-$  centers in diamond are obtained by monitoring photoluminescence intensity while scanning the frequency of the applied microwave pulses [1]. Figure 1c shows typical ODMR spectra of the same nanodiamond, which has a two-dip feature around 2.88 GHz, the value of zero-field splitting of NV centers at cryogenics temperatures. The resonant frequencies and widths are extracted by numerical fitting, and their power dependence is summarized in Fig. 1d. In the weak excitation region, both the splitting and width of the ODMR spectra decrease with laser power. We measured several different NDs, and they all show similar power dependence, see Supplemental Material for details.

To verify whether this observation is a general effect, three other batches of diamond samples are measured. First, ODMR spectra of ensemble NV centers in microdiamonds (MDs) and a bulk diamond (S5), with similar nitrogen concentration (about 200 ppm), are shown in Fig. 2 a-b. The laser power dependence of ODMR splitting and width of these spectra, as summarized in Fig. 2 d-e, are similar to that of NDs, indicating that par-

TABLE I. Details of diamond samples used in this work.

Sample	size	[N]	[NV]
ND	~100 nm	~ 200 ppm	~3 ppm
MD	~ 1 $\mu$ m	~ 200 ppm	~3 ppm
S5	3 $\times$ 3 $\times$ 0.5 mm <sup>3</sup>	~ 200 ppm	5-40 ppm
E6-2	3 $\times$ 3 $\times$ 0.7 mm <sup>3</sup>	14 ppm	~3 ppm

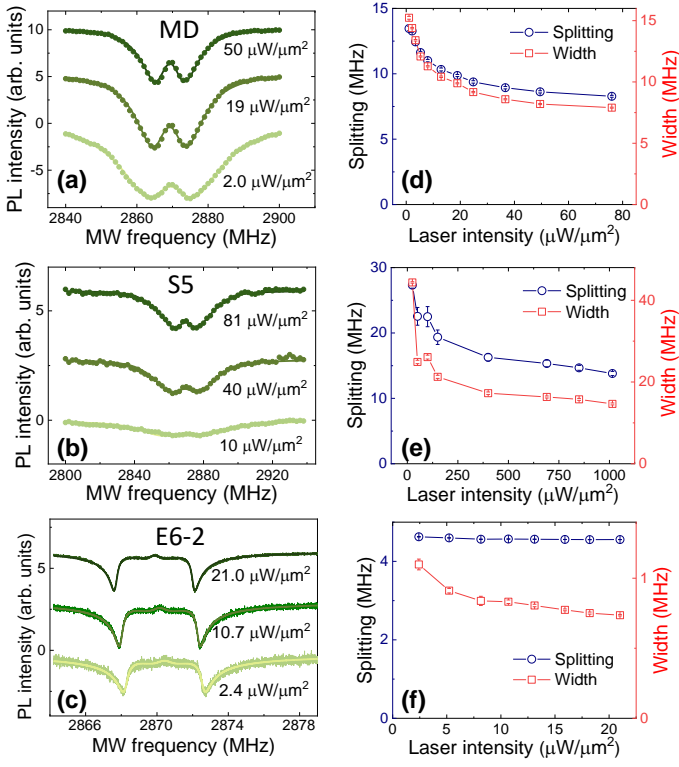


FIG. 2. (a-c) ODMR spectra of NV centers in microdiamonds (MD), and bulk diamonds (S5 and E6-2) under weak laser excitation, see Table I for detailed sample information. (d-e) Laser power dependence of the ODMR splitting and width for the (d) MD sample, (e) S5 sample, and (f) E6-2 sample.

ticle size is not a key factor for this effect.

Second, ODMR spectra of another bulk diamond (E6-2) with similar NV concentration but more dilute N concentrations ( $\sim 14$  ppm) were measured, as shown in Fig. 2c. In this measurement, pairs of coils were used to compensate the background magnetic field in the laboratory. The main feature of these ODMR spectra is the hyperfine splitting caused by the host  $^{14}\text{N}$  nuclear spins. Numerical fitting considering the internal electric field and hyperfine coupling is used to extract ODMR splitting and width. Both parameters decrease slightly with the increase of the applied laser power, as presented in the inset of Fig. 2f.

Summarizing, key features of NV ODMR spectra have unambiguous power dependence in the weak excitation region, and this effect is closely associated with the nitrogen concentration of the diamond sample.

To quantitatively understand these results, we adapt the  $\text{NV}^- - \text{N}^+$  pair model [22] developed by Manson *et al* and pay special attention to the internal electric field around NV centers [21]. Key points of this model are: (1) NV and N defects are randomly distributed in the diamond lattice. (2) Each NV center captures an electron from one of its nearby N atoms and forms an  $\text{NV}^- - \text{N}^+$  pair. (3) Resonance frequencies of each NV center are

determined by its local internal electric field. (4) Upon laser excitation, some of the  $\text{NV}^- - \text{N}^+$  pairs are charge neutralized, resulting in more dilute charge density and smaller internal electric field for the remaining  $\text{NV}^-$  centers.

For simplicity, we assume that an NV center always pairs with its nearby N atoms. The local electric field at the NV position contains two parts, the electric field from its paired  $\text{N}^+$  ion ( $E_N$ ) and the dipole fields ( $E_{\text{dipole}}$ ) from all the other  $\text{NV}^- - \text{N}^+$  pairs. For the nano- and micro-diamond samples, the N concentration ( $\sim 200$  ppm) is much larger than the NV concentration (3 ppm), so the distance between different pairs is much larger than the distance between the two point charges ( $\text{NV}^-$  and its nearby  $\text{N}^+$ ). As a result, the  $E_N$  part dominates the internal electric field and the  $E_{\text{dipole}}$  term can be ignored. Under these conditions, the splitting and width of ODMR spectra of ensemble NV centers can be related to the N concentration (see Supplemental Material for detailed derivation):

$$\begin{aligned} S_{\text{ODMR}} &\approx 0.42 \rho_N^{\frac{2}{3}} \text{ MHz/ppm}^{\frac{2}{3}}, \\ W_{\text{ODMR}} &\approx 0.31 \rho_N^{\frac{2}{3}} \text{ MHz/ppm}^{\frac{2}{3}}. \end{aligned} \quad (1)$$

where  $\rho_N$  is the concentration of the N atoms (in ppm). It is clear that a dense N distribution brings large splitting and broadening features to the ODMR spectra. When the NV and N concentrations are of the same order of magnitude, for example, in the E6-2 sample, both the  $E_N$  and  $E_{\text{dipole}}$  terms should be taken into account, but the nitrogen concentration dependence of ODMR parameters is similar to the former case.

With the model in hand, we now use numerical simulations to investigate the effect of nitrogen density and laser-induced charge neutralization on key features of ODMR spectra. NV centers and N atoms are randomly placed in a sphere of 100-nm diameter, and the total number of NV centers (and Ns) are chosen to match the known defect concentrations. The positions of the  $i$ -th NV center and  $j$ -th N atom are denoted as  $\{\vec{r}_i\}$  and  $\{\vec{r}_j\}$ , respectively. The electric field on the  $i$ -th  $\text{NV}^-$  center is:

$$\vec{E}^i = \frac{-e}{4\pi\epsilon_0\epsilon_r} \left[ \sum_{k \neq i} \frac{\hat{r}_{ki}}{r_{ki}^2} - \sum_j \frac{\hat{r}_{ji}}{r_{ji}^2} \right], \quad (2)$$

where  $\epsilon_0$  is the vacuum permittivity,  $\epsilon_r = 5.7$  is the relative permittivity of diamond [26], and  $r_{ki}$  and  $r_{ji}$  are the distances from the  $k$ -th  $\text{NV}^-$  and  $j$ -th  $\text{N}^+$  to the NV position,  $\hat{r}_{ki}$  and  $\hat{r}_{ji}$  are the corresponding unit vectors.

This electric field can be decomposed into parallel ( $E_z^i$ ) and perpendicular ( $E_{\{x,y\}}^i$ ) components relative to the NV axis, and it couples to the NV electron spin through  $\Pi_{\{x,y\}}^i = d_{\perp} E_{\{x,y\}}^i$  and  $\Pi_z^i = d_{\parallel} E_z^i$ , with susceptibilities  $\{d_{\parallel}, d_{\perp}\} = \{0.35, 17\} \text{ Hz} \cdot \text{cm/V}$  [21, 27]. Specifically, the axial component of the electric field shifts the resonant frequency of the NV center, and the transverse component splits the resonance peaks. It is worth noting that

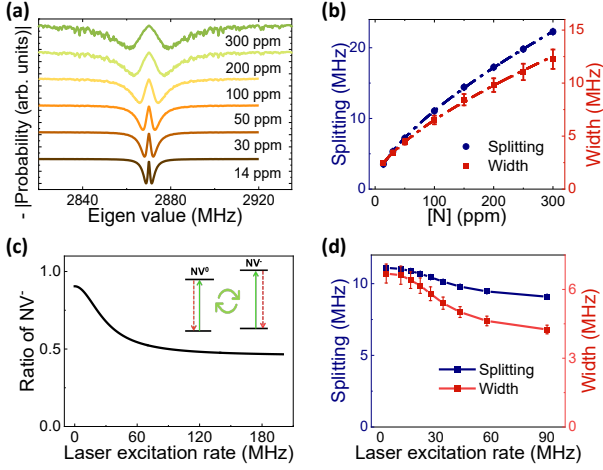


FIG. 3. Numerical results. (a) The probability distribution of NV resonant frequency under different nitrogen concentrations ( $[NV]=3$  ppm). (b) Splitting and width of the numerical spectra as a function of the nitrogen concentration. The dashed lines are fitting results with Eq. 1. (c-d) Laser power dependence of (c) the remnant  $NV^-$  ratio, and (d) splitting and width of the numerical ODMR spectra under various optical excitation rates.  $[N]=100$  ppm and  $[NV]=3$  ppm are used in this simulation.

the coefficient of the transverse component ( $d_{\perp}$ ) is much larger than that of the axial component ( $d_{\parallel}$ ), resulting in the two-dip feature of ensemble NV ODMR spectra.

The NV spin Hamiltonian under the electric field is [8]:

$$H_i = (D_{gs} + \Pi_z^i) S_z^2 + \Pi_x^i (S_y^2 - S_x^2) + \Pi_y^i (S_x S_y + S_y S_x), \quad (3)$$

where the  $D_{gs} = (2\pi) \times 2.87$  GHz is the zero-filed splitting, and  $S$  is the NV spin operator. We have ignored the hyperfine coupling to the host  $^{14}\text{N}$  and nearby  $^{13}\text{C}$  nuclear spins in the calculation, as they are constant and do not change under laser excitation. After diagonalizing the Hamiltonian, the eigenvalues of each NV center and corresponding resonant frequencies are obtained. For a given defect concentration, the calculation was repeated  $10^5$  times, and the resonant frequencies of all NV centers are taken into account to obtain their statistical features.

Figure 3a presents the probability distribution of NV resonant frequency under different N concentrations. Although the intrinsic spin dephasing and technical broadening factors (e.g. microwave power broadening) have not been taken into account, these numerical spectra capture the key features of the experimentally measured ODMR spectra. The numerical results confirm that a dense N distribution brings splitting and broadening to the ODMR spectra, as summarized in Fig. 3b. The numerical results also fit well with the theoretical formula of Eq. 1. As an application of this result, one can use the ODMR splitting and width under zero-field to estimate the nitrogen concentration of unknown diamond samples if the light illumination is sufficiently well characterized.

Next, we show that laser intensity plays an important role in determining the key feature of ODMR spectra in the weak excitation region. First-principle calculation suggests that the energy required for the reaction  $NV^0 + N^0 \Rightarrow NV^- - N^+$  is always negative [28]. Thus,  $NV^- - N^+$  pairs are stable in the dark. Under laser excitation, however, the reverse process can take place, and part of the  $NV^- - N^+$  pairs are charge neutralized. In our measured samples, this is most likely to take place through a one-photon process [29], as weak laser excitation is sufficient to induce this effect. The equilibrium charge state of NV centers under laser excitation can be obtained by solving a master equation that includes both the optical excitation and charge conversion rates, see Supplementary Material for details. As shown in Fig. 3c, the remaining ratio of  $NV^-$  centers decreases with increasing laser power. For the remaining  $NV^-$  centers, we also calculate their ODMR spectra using the above-mentioned method. The laser power dependence of ODMR splitting and width are shown in Fig. 3d. It is clear that the effect of laser-induced charge neutralization becomes more significant in the weak excitation region.

(Discussion) In our numerical simulation, we have used a simplified assumption that an NV center only pairs with its nearest nitrogen atom. In fact, with multiple N atoms available, an NV center could also pair with other nitrogen atoms. Meanwhile, the pair “partner” of a given NV center can also change with time. Nevertheless, the good agreement between the numerical and experimental results suggests that the simplified model captures the key features of laser-induced charge neutralization of  $NV^- - N^+$  pairs. We note that the light narrowing effect could also be explained by the model developed by Jensen *et al* [19], where laser pumping induces “effective” spin relaxation of NV centers and suppresses the microwave power broadening of their magnetic resonance signal. However, the currently observed laser power dependence of ODMR splitting cannot be explained by this spin-only model. We emphasize that the contribution of internal electronic fields becomes most prominent under zero magnetic field, and an external magnetic field could be applied to suppress the broadening and partially recover the magnetic sensitivity of NV-based quantum sensors. For quantum sensing applications, our results suggest that key features of ODMR spectra can be modified by laser power, thus it is crucial to maintain a stable laser power in sensing applications.

In summary, we experimentally observe unambiguous laser-power dependence of zero-field ODMR spectra of NV ensemble in nano-, micro-, and bulk diamonds. In the weak-excitation regime, both the width and splitting of the ODMR lines decrease with increasing laser power, which is accompanied by a reversible change of the  $NV^-$  ZPL peak height. We adopt the  $NV^- - N^+$  pair model and carry out numerical simulations to verify the effect of laser-induced charge neutralization. It turns out that both the laser power and the nitrogen-concentration dependence can be well understood with this simple model.

These results will be useful in diamond-based quantum sensing applications, for example, probing biological intracellular signals and in studies of temperature-sensitive thin-film materials.

## ACKNOWLEDGEMENTS

The authors acknowledge helpful discussions with Neil Manson and Till Lenz. This work was supported by the Natural Science Foundation of Beijing, China (Grant No. Z200009), the National Key Re-

search and Development Program of China (Grants No. 2019YFA0308100), the Chinese Academy of Sciences (Grant Nos. YJKYYQ20190082, XDB28030000, XDB33000000), and the National Natural Science Foundation of China (Grant Nos. 11974020, 12022509, 11934018, T2121001). Q. L. and R.-B.L. acknowledge the funding support from Hong Kong Research Grants Council - Collaborative Research Fund under project no. C4007-19G. The work of DB was supported by the European Commission's Horizon Europe Framework Program under the Research and Innovation Action MUQUABIS GA no. 101070546.

- 
- [1] A. Gruber, A. Drabenstedt, C. Tietz, L. Fleury, J. Wrachtrup, and C. v. Borczyskowski, Scanning confocal optical microscopy and magnetic resonance on single defect centers, *Science* **276**, 1212 (1997).
  - [2] G. Balasubramanian, I. Chan, R. Kolesov, M. Al-Hmoud, J. Tisler, C. Shin, C. Kim, A. Wojcik, P. R. Hemmer, A. Krueger, *et al.*, Nanoscale imaging magnetometry with diamond spins under ambient conditions, *Nature* **455**, 648 (2008).
  - [3] J. Maze, P. Stanwix, J. Hodges, S. Hong, J. Taylor, P. Cappellaro, L. Jiang, M. G. Dutt, E. Togan, A. Zibrov, *et al.*, Nanoscale magnetic sensing with an individual electronic spin in diamond, *Nature* **455**, 644 (2008).
  - [4] J. Taylor, P. Cappellaro, L. Childress, L. Jiang, D. Budker, P. Hemmer, A. Yacoby, R. Walsworth, and M. Lukin, High-sensitivity diamond magnetometer with nanoscale resolution, *Nature Physics* **4**, 810 (2008).
  - [5] V. M. Acosta, E. Bauch, M. P. Ledbetter, A. Waxman, L.-S. Bouchard, and D. Budker, Temperature dependence of the nitrogen-vacancy magnetic resonance in diamond, *Phys. Rev. Lett.* **104**, 070801 (2010).
  - [6] X.-D. Chen, C.-H. Dong, F.-W. Sun, C.-L. Zou, J.-M. Cui, Z.-F. Han, and G.-C. Guo, Temperature dependent energy level shifts of nitrogen-vacancy centers in diamond, *Applied Physics Letters* **99**, 161903 (2011).
  - [7] M. W. Doherty, V. V. Struzhkin, D. A. Simpson, L. P. McGuinness, Y. Meng, A. Stacey, T. J. Karle, R. J. Hemley, N. B. Manson, L. C. Hollenberg, *et al.*, Electronic properties and metrology applications of the diamond nv- center under pressure, *Phys. Rev. Lett.* **112**, 047601 (2014).
  - [8] F. Dolde, H. Fedder, M. W. Doherty, T. Nobauer, F. Rempp, G. Balasubramanian, T. Wolf, F. Reinhard, L. C. L. Hollenberg, F. Jelezko, and J. Wrachtrup, Electric-field sensing using single diamond spins, *Nature Physics Letter* **455**, 644 (2008).
  - [9] R. Schirhagl, K. Chang, M. Loretz, and C. L. Degen, Nitrogen-vacancy centers in diamond: nanoscale sensors for physics and biology, *Annual review of physical chemistry* **65**, 83 (2014).
  - [10] J.-H. Dai, Y.-X. Shang, Y.-H. Yu, Y. Xu, H. Yu, F. Hong, X.-H. Yu, X.-Y. Pan, and G.-Q. Liu, Optically detected magnetic resonance of diamond nitrogen-vacancy centers under megabar pressures, *Chinese Physics Letters* **39**, 117601 (2022).
  - [11] P. J. Scheidegger, S. Diesch, M. L. Palm, and C. Degen, Scanning nitrogen-vacancy magnetometry down to 350 mk, *Applied Physics Letters* **120**, 224001 (2022).
  - [12] P. P. Laissue, R. A. Alghamdi, P. Tomancak, E. G. Reynaud, and H. Shroff, Assessing phototoxicity in live fluorescence imaging, *Nature methods* **14**, 657 (2017).
  - [13] X. Feng, W.-H. Leong, K. Xia, C.-F. Liu, G.-Q. Liu, T. Rendler, J. Wrachtrup, R.-B. Liu, and Q. Li, Association of nanodiamond rotation dynamics with cell activities by translation-rotation tracking, *Nano Letters* **21**, 3393 (2021).
  - [14] C. Grezes, B. Julsgaard, Y. Kubo, M. Stern, T. Umeda, J. Isoya, H. Sumiya, H. Abe, S. Onoda, T. Ohshima, V. Jacques, J. Esteve, D. Vion, D. Esteve, K. Mølmer, and P. Bertet, Multimode storage and retrieval of microwave fields in a spin ensemble, *Phys. Rev. X* **4**, 021049 (2014).
  - [15] S. E. Lillie, D. A. Broadway, N. Donschuk, S. C. Scholten, B. C. Johnson, S. Wolf, S. Rachel, L. C. Hollenberg, and J.-P. Tetienne, Laser modulation of superconductivity in a cryogenic wide-field nitrogen-vacancy microscope, *Nano Letters* **20**, 1855 (2020).
  - [16] V. M. Acosta, L. S. Bouchard, D. Budker, R. Folman, T. Lenz, P. Maletinsky, D. Rohner, Y. Schlusser, and L. Thiel, Color centers in diamond as novel probes of superconductivity, *Journal of Superconductivity and Novel Magnetism* **32**, 85 (2019).
  - [17] Y. Schlusser, T. Lenz, D. Rohner, Y. Bar-Haim, L. Bougas, D. Groswasser, M. Kieschnick, E. Rozenberg, L. Thiel, A. Waxman, *et al.*, Wide-field imaging of superconductor vortices with electron spins in diamond, *Physical Review Applied* **10**, 034032 (2018).
  - [18] J. Choi, H. Zhou, R. Landig, H.-Y. Wu, X. Yu, S. E. Von Stetina, G. Kucsko, S. E. Mango, D. J. Needleman, A. D. Samuel, *et al.*, Probing and manipulating embryogenesis via nanoscale thermometry and temperature control, *Proceedings of the National Academy of Sciences* **117**, 14636 (2020).
  - [19] K. Jensen, V. M. Acosta, A. Jarmola, and D. Budker, Light narrowing of magnetic resonances in ensembles of nitrogen-vacancy centers in diamond, *Phys. Rev. B* **87**, 014115 (2013).
  - [20] N. Aslam, G. Waldherr, P. Neumann, F. Jelezko, and J. Wrachtrup, Photo-induced ionization dynamics of the nitrogen vacancy defect in diamond investigated by single-shot charge state detection, *New Journal of*

- Physics **15**, 013064 (2013).
- [21] T. Mittiga, S. Hsieh, C. Zu, B. Kobrin, F. Machado, P. Bhattacharyya, N. Rui, A. Jarmola, S. Choi, D. Budker, *et al.*, Imaging the local charge environment of nitrogen-vacancy centers in diamond, *Phys. Rev. Lett.* **121**, 246402 (2018).
  - [22] N. B. Manson, M. Hedges, M. S. Barson, R. Ahlefeldt, M. W. Doherty, H. Abe, T. Ohshima, and M. J. Sellars, NV—N<sup>+</sup> pair centre in 1b diamond, *New J. Phys* **20**, 113037 (2018).
  - [23] S. Baier, C. E. Bradley, T. Middelburg, V. V. Dobrovitski, T. H. Taminiau, and R. Hanson, Orbital and spin dynamics of single neutrally-charged nitrogen-vacancy centers in diamond, *Phys. Rev. Lett.* **125**, 193601 (2020).
  - [24] S. Dhomkar, H. Jayakumar, P. R. Zangara, and C. A. Meriles, Charge dynamics in near-surface, variable-density ensembles of nitrogen-vacancy centers in diamond, *Nano letters* **18**, 4046 (2018).
  - [25] I. C. Barbosa, J. Gutsche, and A. Widera, Impact of charge conversion on nv-center relaxometry, *arXiv preprint arXiv:2301.01063* (2023).
  - [26] S. Whitehead and W. Hackett, Measurement of the specific inductive capacity of diamonds by the method of mixtures, *Proceedings of the Physical Society* (1926-1948) **51**, 173 (1939).
  - [27] E. Van Oort and M. Glasbeek, Electric-field-induced modulation of spin echoes of nv centers in diamond, *Chemical Physics Letters* **168**, 529 (1990).
  - [28] A. M. Ferrari, K. E. El-Kelany, F. S. Gentile, M. D’Amore, and R. Dovesi, The nv- n<sup>+</sup> charged pair in diamond: a quantum-mechanical investigation, *Physical Chemistry Chemical Physics* **23**, 18724 (2021).
  - [29] R. Löfgren, S. Öberg, and J. Larsson, A theoretical study of de-charging excitations of the nv-center in diamond involving a nitrogen donor, *New Journal of Physics* **22**, 123042 (2020).



# Supplemental Information: Power Dependence of Optically Detected Magnetic Resonance with Nitrogen-Vacancy Centers in Diamond under Weak Laser Excitation

Yong-Hong Yu,<sup>1,2</sup> Rui-Zhi Zhang,<sup>1,2</sup> Yue Xu,<sup>1,2</sup> Huijie Zheng,<sup>1,3,\*</sup> Quan Li,<sup>4</sup>  
Ren-Bao Liu,<sup>4</sup> Xin-Yu Pan,<sup>1,3,5</sup> Dmitry Budker,<sup>6,7,8</sup> and Gang-Qin Liu<sup>1,3,5,†</sup>

<sup>1</sup>*Beijing National Laboratory for Condensed Matter Physics,  
Institute of Physics, Chinese Academy of Sciences, Beijing 100190, China*

<sup>2</sup>*School of Physical Sciences, University of Chinese Academy of Sciences, Beijing 100049, China*

<sup>3</sup>*Songshan Lake Materials Laboratory, Dongguan, Guangdong 523808, China*

<sup>4</sup>*Department of Physics, Centre for Quantum Coherence,  
and The Hong Kong Institute of Quantum Information Science and Technology,  
The Chinese University of Hong Kong, New Territories, Hong Kong, China*

<sup>5</sup>*CAS Center of Excellence in Topological Quantum Computation, Beijing 100190, China*

<sup>6</sup>*Johannes Gutenberg-Universität Mainz, 55128 Mainz, Germany*

<sup>7</sup>*Helmholtz-Institut, GSI Helmholtzzentrum für Schwerionenforschung, 55128 Mainz, Germany*

<sup>8</sup>*Department of Physics, University of California, Berkeley, California 94720, USA*

## CONTENTS

I. Experimental setup and sample preparation	2
II. Theoretical model and numerical fitting	3
A. Probability distribution of the nearest NV <sup>-</sup> and N pairs	3
B. Analytical derivation of the ODMR spectra	4
C. Fitting function for the ODMR spectra	4
III. Numerical simulation of ensemble NV ODMR	5
A. Nitrogen concentration dependence	6
B. Laser power dependence	6
IV. Extended data: ODMR of nanodiamonds and microdiamonds	8
References	10

---

\* [hjzheng@iphy.ac.cn](mailto:hjzheng@iphy.ac.cn)

† [gqliu@iphy.ac.cn](mailto:gqliu@iphy.ac.cn)

## I. EXPERIMENTAL SETUP AND SAMPLE PREPARATION

The ODMR and PL measurements of nanodiamonds, microdiamonds, and sample S5 (bulk diamond) are carried out on home-built confocal microscopies. The light source is a continuous-wave 532 nm laser (CNI, MLL-III-532-150 mW), and the laser power can be adjusted by neutral density filters (Thorlabs) right after the laser. An objective with a 0.9 numerical aperture is used to focus the laser beam onto diamond samples and also collect the NV fluorescence. The focal spot is estimated to have a waist of 1  $\mu\text{m}$ . Confocal images of the diamond samples are obtained by scanning either the sample holder (using piezoelectric stages) or the incident laser beam (using galvo mirrors).

ODMR spectra are measured by recording fluorescence (between 650 nm to 800 nm) photon counts of the NV centers as a function of the driving microwave (MW) frequency. Microwaves are generated by signal generators (Rohde & Schwarz SMIQ06B, or Keysight N5183B), through an RF switch (Mini-Circuits, ZASWA-2-50DR+), then amplified by a high-power amplifier (Mini-Circuits, ZHL-16W-43-s+), and delivered to the antenna (a twenty-micron silver wire) on the sample holder. No external magnetic field is applied in all the ODMR measurements. For the E6-2 sample, a set of three-dimension Helmholtz coils is used to compensate the geomagnetic field, since the splitting due to the internal electrical field is small (less than 1 MHz).

Nanodiamonds (NDs) and microdiamonds (MDs) containing ensemble NV centers are purchased from Adámas Nanotechnologies. These crystals are supplied in deionized water at a mass concentration of 1 mg/mL. After being diluted with isopropanol and ultrasonic treatment, a drop of 5  $\mu\text{L}$  ND isopropanol solution (2.5  $\mu\text{g}/\text{mL}$ ) is transferred to a substrate (STO or  $\text{Al}_2\text{O}_3$ ) with a pipette. Nanodiamonds are deposited on the substrate after the volatilization of the isopropanol. Fig. S1 (a) shows a typical confocal scanning image of nanodiamonds samples.

To estimate the laser excitation efficiency of the confocal system, we measured the laser power dependence of the NV fluorescence counts, and the results are shown in Fig. S1 (b). The saturation power is more than 1 mW of (5000  $\mu\text{W}/\mu\text{m}^2$  in intensity). In the same figure, we also plot the ratio of ZPL peaks of  $\text{NV}^-$  (637 nm) and  $\text{NV}^0$  (575 nm). It indicates that a laser-induced charge neutralization effect is prominent in the condition of weak excitation (one or more order weaker than the saturation power).

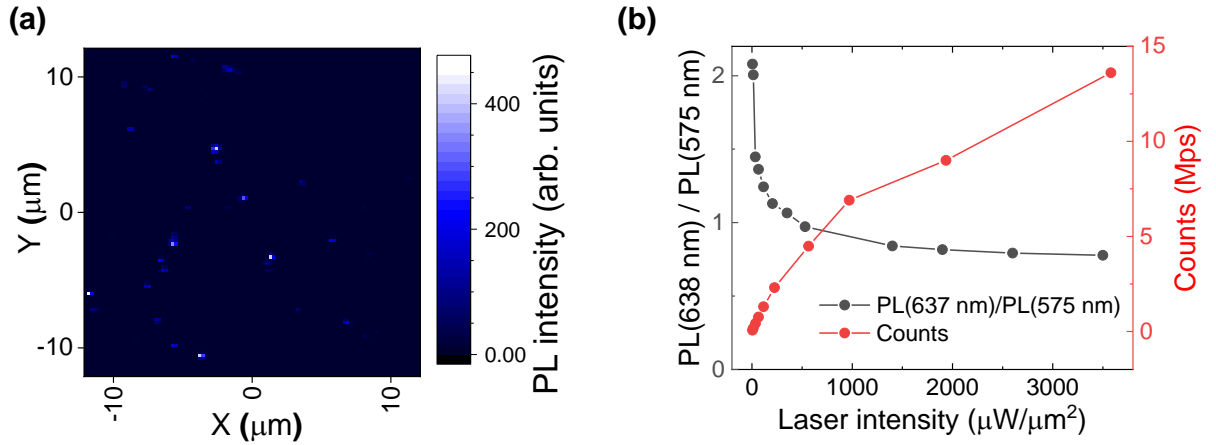


FIG. S1. (a) Confocal image of nanodiamonds on  $\text{Al}_2\text{O}_3$  substrate. (b) Laser power dependence of NV fluorescence counts and the ratio of ZPL peaks between  $\text{NV}^-$  (637 nm) and  $\text{NV}^0$  (575 nm). The data are from the same ND shown in Fig. 1 of the main text.



## II. THEORETICAL MODEL AND NUMERICAL FITTING

We adopt the  $\text{NV}^- - \text{N}^+$  pair model [1, 2] to explain the observed laser power dependence of ODMR spectra. The key point of our model is that each NV center captures an electron from one of its nearby nitrogen (N) atoms and forms an  $\text{NV}^- - \text{N}^+$  pair. The randomly distributed charges in the diamond lattice ( $\text{NV}^-$ ,  $\text{N}^+$ , and other charge traps) bring a local electric field to each  $\text{NV}^-$  center, which brings about observable effects on the PL and ODMR signals. For a given local electric field at the position of the  $\text{NV}^-$  center,  $\vec{E}$ , couples with the spin of the  $\text{NV}^-$  center via the Hamiltonian:

$$\hat{H} = (D_{gs} + \Pi_z) S_z^2 + \Pi_x (S_y^2 - S_x^2) + \Pi_y (S_x S_y + S_y S_x), \quad (1)$$

where  $D_{gs} = 2870$  MHz is the zero-field splitting of an  $\text{NV}^-$  center,  $S$  are the electronic spin-1 operators of the  $\text{NV}^-$  center, The terms  $\Pi_{\{x,y\}} = d_{\perp} E_{\{x,y\}}$  and  $\Pi_z = d_{\parallel} E_z$  characterize the coupling between the  $\text{NV}^-$ 's electronic spin and its surrounding electric field,  $\vec{E}$ , with susceptibilities  $\{d_{\parallel}, d_{\perp}\} = \{0.35, 17\}$  Hz · cm/V [3]. We ignore the parallel component of the electric field in the following discussion, as its contribution is about two orders smaller than the perpendicular components. The eigenvalues of this Hamiltonian are  $\varepsilon^{\pm} = D_{gs} \pm \Pi_{\perp}$  and  $\varepsilon^0 = 0$ .

In this section, we first derive the probability distribution of the distance between  $\text{NV}^- - \text{N}^+$  pairs, and then use this result to calculate the internal electric field of  $\text{NV}^-$  centers in diamond. We obtain the formula to fit the experimental ODMR spectra at the end of this section.

### A. Probability distribution of the nearest $\text{NV}^-$ and N pairs

This subsection provides a mathematical model for the probability of finding nitrogen atoms at a certain distance ( $r$ ) from an NV center. To simplify the derivation procedure, we suppose an NV center is located at the center of a diamond sphere. There are total  $N$  nitrogen atoms in the sphere and its volume is  $V$ .  $P(r)dr$  is the probability to find a nitrogen atom at a distance between  $r$  and  $r + dr$  from the NV center. As the nitrogen atoms are randomly distributed in the diamond lattice,  $P(r)dr$  is proportional to the volume of a thin spherical shell of thickness  $dr$  and radius  $r$ , which is  $4\pi r^2 dr/V$ . Meanwhile, the probability of a nitrogen atom at a distance larger than  $r$  is  $(V - \frac{4}{3}\pi r^3)/V$ . Using these formulae, we can write  $P(r)dr$  as:

$$P(r)dr = \sum_{i=1}^N C_N^i \left( \frac{4\pi r^2 dr}{V} \right)^i \left( \frac{V - \frac{4}{3}\pi r^3}{V} \right)^{N-i}, \quad (2)$$

where  $C_N^i$  is the binomial coefficient, representing the number of ways to choose  $i$  nitrogen atoms from a total number  $N$ , which is calculated as following,

$$N = n'_0 \cdot \rho_N \cdot V, \quad (3)$$

where  $\rho_N$  is the nitrogen concentration in ppm,  $n'_0 = 1.76 \times 10^{-4}$  (ppm·nm<sup>3</sup>)<sup>-1</sup> is the factor relating the number density (in ppm) to the volume density. Now we take  $n_0 = 1/2 n'_0$  for the consideration of the number of atoms in a primitive cell. For a normal NV diamond sample,  $V \cdot n_0 \gg 1$ . Thus, we can simplify the expression of  $P(r)$  as:

$$P(r) = 8\pi \rho_N n_0 r^2 \exp\left(-\frac{8}{3}\pi \rho_N n_0 r^3\right). \quad (4)$$

The average distance between the NV center and its nearest nitrogen atom can be calculated as :

$$\langle r \rangle = \int_0^{\infty} r P(r) dr = \left( \frac{3}{8\pi} \right)^{1/3} \Gamma[4/3] (\rho_N n_0)^{1/3}, \quad (5)$$

where  $\Gamma[z+1]$  is the Gamma function defined as  $\Gamma[z+1] = \int_0^{\infty} \mu^z \exp(-\mu) d\mu$ .

In addition to the average distance, we can calculate the standard deviation of the distribution. The standard deviation,  $\sigma_r$ , is given by:

$$\sigma_r = \sqrt{\langle r^2 \rangle - \langle r \rangle^2} = \left( \frac{3}{8\pi} \right)^{1/3} \sqrt{\Gamma[5/3] - \Gamma[4/3]^2} (\rho_N n_0)^{-1/3}. \quad (6)$$

### B. Analytical derivation of the ODMR spectra

We assume that an NV center always pairs with its nearest nitrogen atom. Under this assumption, the probability of an  $NV^- - N^+$  pair has a distance  $r$  is the same as Eq.(4). For the case of  $\rho_N \gg \rho_{NV}$ , that is, when the nitrogen concentration is much larger than that of the NV concentration, the distance between the paired  $NV^-$  and  $N^+$  is much smaller than the distance between two adjacent pairs. Therefore, the local electric field at the  $NV^-$  position is dominated by the field generated by the paired  $N^+$  atom ( $E_N$ ), and the probability distribution of  $E_N$  can be derived using the differential relation  $F_1(E_N) dE_N = P_1(r) dr$ :

$$F_1(E_N) = -\frac{4\pi\rho_N n_0 \alpha^3}{E_N^{5/2}} \exp\left(-\frac{8\pi\rho_N n_0 \alpha^3}{3E_N^{3/2}}\right), \quad (7)$$

where  $\alpha = \left(\frac{e}{4\pi\epsilon_0\epsilon_r}\right)^{1/2}$ ,  $\epsilon_0$  is the vacuum permittivity,  $\epsilon_r = 5.7$  is the relative permittivity of diamond [4].

The relationship between the resonant frequency of an  $NV^-$  center and its local electric field is:

$$|v' - D_{gs}| = d_\perp E_\perp = \frac{\sqrt{6}}{3} d_\perp E_\perp. \quad (8)$$

The coefficient  $\frac{\sqrt{6}}{3}$  is used to re-scale the strength of the electric field considering the random orientation of the internal electric field. Using this relation, the distribution of  $F_1(E_N)$  gives the ODMR spectrum of:

$$g_1(v) = -\frac{4\pi\rho_N n_0 \alpha'^3}{|v - D_{gs}|^{5/2}} \exp\left(-\frac{8\pi\rho_N n_0 \alpha'^3}{3|v - D_{gs}|^{3/2}}\right), \quad (9)$$

where  $\alpha' = \left(\frac{\sqrt{6}}{3} d_\perp\right)^{1/2} \alpha$ . It is easy to derive the splitting ( $S_1$ ) and the width ( $W_1$ ) of  $g_1(v)$ , which are:

$$\begin{aligned} S_1 &= 2 \left(\frac{8}{5}\pi n_0 \alpha'^3\right)^{2/3} \rho_N^{2/3}, \\ W_1 &= 1.463 \left(\frac{8}{5}\pi n_0 \alpha'^3\right)^{2/3} \rho_N^{2/3}. \end{aligned} \quad (10)$$

Considering the relevant parameters of  $NV^-$  center, we can get:

$$\begin{aligned} S_1 &= 0.42 \rho_N^{2/3} \text{ MHz/ppm}^{2/3}, \\ W_1 &= 0.31 \rho_N^{2/3} \text{ MHz/ppm}^{2/3}. \end{aligned} \quad (11)$$

The above derivation shows that when  $\rho_N \gg \rho_{NV}$ , the splitting and width of the NV ODMR spectra are mainly determined by the nitrogen concentration and have little dependence on the  $NV^-$  concentration. Note that in the present approach, the nearest  $N^+$  tends to be close to an  $NV^-$ . This is different from the approximation used in [2] where random distributions over the crystal were assumed.

### C. Fitting function for the ODMR spectra

For the E6-2 sample,  $\rho_{NV}$  is close to  $\rho_N$ , and the distance between two  $NV^-$  centers is comparable to that between  $NV^-$  and the nearest  $N^+$ . In this situation, the electric field generated by nearby  $NV^- - N^+$  pairs ( $E_{dipole}$ ) should also be taken into account. The nearest pair can be considered as a dipole with a distance  $r_2$  from the NV center, and the probability distribution of  $E_{dipole}$  can be derived using the differential relation  $F_2(E_{dipole}) dE_{dipole} = P_2(r_2) dr_2$ :

$$F_2(E_{dipole}) = -\frac{8\pi\rho_{NV} n_0 \beta^3}{3E_{dipole}^2 \rho_N^{1/3}} \exp\left(-\frac{8\pi\rho_{NV} n_0 \beta^3}{3E_{dipole} \rho_N^{1/3}}\right), \quad (12)$$

where  $\beta = \left(\frac{2\Gamma(4/3)e}{4\pi\epsilon_0\epsilon_r}\right)^{1/3} \left(\frac{8}{3}\pi n_0\right)^{-1/9}$ . Similarly, the distribution of  $F_2(E_{dipole})$  corresponds to ODMR spectra given by  $E_{dipole}$ :

$$g_2(v) = -\frac{8\pi\rho_{NV} n_0 \beta'^3}{3|v - D_{gs}|^2 \rho_N^{1/3}} \exp\left(-\frac{8\pi\rho_{NV} n_0 \beta'^3}{3|v - D_{gs}| \rho_N^{1/3}}\right), \quad (13)$$

where  $\beta' = \left(\frac{\sqrt{6}}{3}d_{\perp}\right)^{1/3}\beta$ . The total electric field  $E_{total}$  is the vector sum of  $E_N$  and  $E_{dipole}$ , and can be expressed as:

$$E_{total} = \sqrt{E_N^2 + E_{dipole}^2 + 2E_N E_{dipole} \cos \Omega}, \quad (14)$$

where  $\Omega$  is the angle between these two vectors. Thus, we have

$$F(E) = \frac{d}{dE} \int_0^{2\pi} \left( \iint_{0 \leq E_{total} \leq E} F_1 F_2 dE_N dE_{dipole} \right) \frac{d\Omega}{2\pi} \sim F_1(E) * F_2(E). \quad (15)$$

The total  $g(v)$  (ignoring laser broadening and natural broadening) is also a nonlinear convolution of the two spectra  $g_1(v)$  and  $g_2(v)$ :

$$g(v) \sim g_1(v) * g_2(v). \quad (16)$$

By observing Eq.(9) and Eq.(13), we can find that  $g_1(v)$  and  $g_2(v)$  have the same mathematical form:

$$g_i(\Pi_{\perp}) \propto -\Pi_{\perp}^{-n_i} \exp(-k_i \Pi_{\perp}^{-n_i+1}). \quad (17)$$

Here,  $2\Pi_{\perp} = 2d_{\perp}E_{\perp}$  indicates the splitting due to electric field. After the convolution  $g_1$  and  $g_2$ , the result spectrum should maintain the original form:

$$g(\Pi_{\perp}) \propto -\Pi_{\perp}^{-n} \exp(-k\Pi_{\perp}^{-n+1}). \quad (18)$$

For a single  $NV^{-}$  center, the ODMR spectrum is determined by both its intrinsic (limited by spin dephasing time) and experimental broadening (power broadening of laser and MW):

$$s(v, \Pi_{\perp}) = \left( \frac{C}{1 + \left(\frac{v - \varepsilon^+}{\delta}\right)^2} + \frac{C}{1 + \left(\frac{v - \varepsilon^-}{\delta}\right)^2} \right). \quad (19)$$

Here, the  $\Pi_{\perp}$  is a variable, which satisfies  $g(\Pi_{\perp})$ . The experimental ODMR spectra of ensemble NV centers are then denoted as:

$$\begin{aligned} G(v) &= \int_0^{+\infty} s(v, \Pi_{\perp}) g(\Pi_{\perp}) d\Pi_{\perp} + C_0 \\ &= C \left( \int_0^{+\infty} \frac{\Pi_{\perp}^{-n} \exp(-k\Pi_{\perp}^{-n+1})}{1 + \left(\frac{v - D_{gs} - \Pi_{\perp}}{\delta}\right)^2} d\Pi_{\perp} + \int_0^{+\infty} \frac{\Pi_{\perp}^{-n} \exp(-k\Pi_{\perp}^{-n+1})}{1 + \left(\frac{v - D_{gs} + \Pi_{\perp}}{\delta}\right)^2} d\Pi_{\perp} \right) + C_0, \end{aligned} \quad (20)$$

where  $C_0$  is a offset.

Considering the nuclear spin of the host  $^{14}\text{N}$ , we add the hyperfine term to the original Hamiltonian:

$$\hat{H} = (D_{gs} + \Pi_z) S_z^2 + \Pi_x (S_y^2 - S_x^2) + \Pi_y (S_x S_y + S_y S_x) + A_{zz} I_z S_z, \quad (21)$$

here,  $I$  is the nuclear spin operator. The energy level is further splitted by:  $\varepsilon_1^{\pm} = D_{gs} \pm \Pi_{\perp}$ ,  $\varepsilon_2^{\pm} = D_{gs} \pm \sqrt{\Pi_{\perp}^2 + A_{zz}^2}$ . The formula of ODMR spectra becomes:

$$\begin{aligned} G(v) &= C_1 \left( \int_0^{+\infty} \frac{\Pi_{\perp}^{-n} \exp(-k_1 \Pi_{\perp}^{-n+1})}{1 + \left(\frac{v - D_{gs} - \Pi_{\perp}}{\delta_1}\right)^2} d\Pi_{\perp} + \int_0^{+\infty} \frac{\Pi_{\perp}^{-n} \exp(-k_1 \Pi_{\perp}^{-n+1})}{1 + \left(\frac{v - D_{gs} + \Pi_{\perp}}{\delta_1}\right)^2} d\Pi_{\perp} \right) \\ &+ C_2 \left( \int_0^{+\infty} \frac{\Pi_{\perp}^{-m} \exp(-k_2 \Pi_{\perp}^{-m+1})}{1 + \left(\frac{v - D_{gs} - \sqrt{\Pi_{\perp}^2 + A_{zz}^2}}{\delta_2}\right)^2} d\Pi_{\perp} + \int_0^{+\infty} \frac{\Pi_{\perp}^{-m} \exp(-k_2 \Pi_{\perp}^{-m+1})}{1 + \left(\frac{v - D_{gs} + \sqrt{\Pi_{\perp}^2 + A_{zz}^2}}{\delta_2}\right)^2} d\Pi_{\perp} \right) + C_B. \end{aligned} \quad (22)$$

### III. NUMERICAL SIMULATION OF ENSEMBLE NV ODMR

In this section, taking nitrogen concentration as a parameter, we use numerical simulation to reproduce the ODMR spectra of ensemble NV centers in diamond.

### A. Nitrogen concentration dependence

The simulation is carried out for a diamond sphere with a diameter of 100 nm. The  $[NV^-]$  concentration is set as 3 ppm. We list the step-by-step procedures below:

1. Calculation of the numbers of NV and N in the given volume. In this simulation, there are  $7.93 \times 10^7$  carbon atoms,  $7.93 \times 10^3$  nitrogen (N), and 238 NV centers.
2. Distribution of N and NV centers in the lattice: The NV centers and N atoms are randomly distributed throughout the 100-nm sphere. It is worth noting that if one defect coincides in the same primitive cell with another, the point will be removed and recalculated until the total number of defects are generated in discrete positions.
3. Formation of  $NV^-$ - $N^+$  pairs: we assume that an NV center always pairs with its nearest N atom and forms an  $NV^-$ - $N^+$  pair. We denote the position of the  $i$ -th  $NV^-$  and  $j$ -th  $N^+$  in by  $\{\vec{r}_i\}$  and  $\{\vec{r}_j\}$ , respectively.
4. Calculation of the internal electric field: for each  $NV^-$  center, its local electric field is the vector sum of all the electric fields from all the other charges:

$$\vec{E}^i = \sum_{k \neq i} \frac{-e}{4\pi\epsilon_0\epsilon_r} \frac{\hat{r}_{ki}}{r_{ki}^2} + \sum_j \frac{e}{4\pi\epsilon_0\epsilon_r} \frac{\hat{r}_{ji}}{r_{ji}^2}, \quad (23)$$

where,  $r_{ki}$  and  $r_{ji}$  are the distances from the  $k$ -th  $NV^-$  and  $j$ -th  $N^+$  to the  $i$ -th  $NV^-$ , respectively;  $\hat{r}_{ki}$ , and  $\hat{r}_{ji}$  are the unit vectors for  $r_{ki}$  and  $r_{ji}$ , respectively.

5. Diagonalization of the Hamiltonian: the presence of a local electric field at the position of the  $i$ -th  $NV^-$  center couple to its spin via the Hamiltonian given by Eq. (1). The Hamiltonian of each  $NV^-$  center is diagonalized, and its three eigenvalues are recorded.
6. Repeat steps 2-5 10,000 times.
7. The probability distribution of the  $NV^-$ - $N^+$  pairs: the probability distribution of the distance between  $NV^-$ - $N^+$  pairs are examined with varying nitrogen concentrations and presented in Fig. S2. Specifically, The inset Fig. S2 depicts the distribution probability of the distance between the  $NV^-$ - $N^+$  pairs in the sample with  $[N]=100$  ppm and  $[NV]=3$  ppm, while the red line represents the distribution probability fitted using Eq. (4).
8. Distribution of eigenvalues is counted and normalized (0-1). For comparison with the ODMR spectra takes into account the sign, i.e., that ODMR corresponds to a decrease in photoluminescence.

The simulation results for samples with different nitrogen concentrations are shown in Fi3(a-b) in the main text.

### B. Laser power dependence

The photo-induced charge conversion of NV centers has been extensively investigated [5–11]. In our model, we use five levels to describe the  $NV^-$  spin states, which include two ground states ( $|1\rangle$  and  $|2\rangle$ ), two excited states ( $|4\rangle$  and  $|5\rangle$ ), and one “effective” singlet state ( $|3\rangle$ ). This model also includes the ground and excited states of  $NV^0$  ( $|6\rangle$  and  $|7\rangle$ ). We use  $\gamma_{ij}$  to represent the rate of spontaneous emission from energy level  $|i\rangle$  to energy level  $|j\rangle$ , as shown in Fig. S3 (a). We define the  $\Gamma_{ion} = \gamma_{56} + \gamma_{46}$ ,  $\Gamma_{rec} = \gamma_{72} + \gamma_{71}$ , and  $\Gamma_{PL} = \gamma_{52} + \gamma_{51} + \gamma_{76}$  as the ionization, recombination and photoluminescence rates, respectively. The values of these parameters are listed in Table I.

We assume that the laser excitation rate is the same for  $NV^-$  and  $NV^0$ . This composite system can be described by the Lindblad master equation [12]:

$$\dot{\rho} = \frac{1}{i\hbar} [H, \rho] + \sum_{\langle ij \rangle} \gamma_{ij} \left( L_{ij} \rho L_{ij}^\dagger - \frac{1}{2} \{ L_{ij}^\dagger L_{ij}, \rho \} \right), \quad (24)$$

where  $\rho$  is the density matrix of the composite system,  $H = L_{532}(|4\rangle\langle 1| + |7\rangle\langle 6| + |5\rangle\langle 2| + h.c.)$  is the Hamiltonian of the composite system with the laser excitation rate ( $L_{532}$ ) in the interaction picture,  $L_{ij} = |j\rangle\langle i|$  is a set of operators describing the dissipating part of the dynamics with the rate  $\gamma_{ij}$ . With these equations, we perform numerical

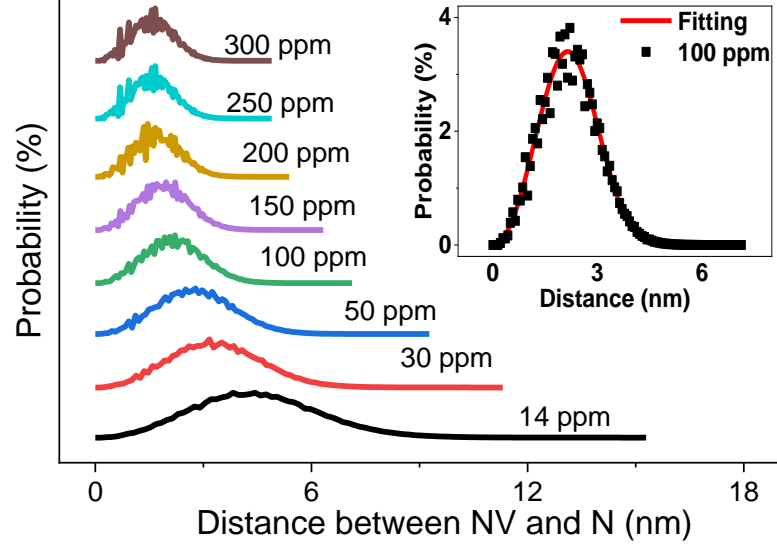


FIG. S2. The probability distribution of the distance of  $\text{NV}^-$ - $\text{N}^+$  pair under different nitrogen concentrations. Insert: For  $[\text{N}]=100$  ppm,  $[\text{NV}]=3$  ppm, the probability distribution of the distance of  $\text{NV}^-$ - $\text{N}^+$  pair and fitting as Eq. (4).

TABLE I. Parameters used in the numerical simulation of laser power dependence, most of the values are taken from [7, 10].

Parameter	Rate (MHz)	Parameter	Rate (MHz)
$\gamma_{41}$	80	$\gamma_{52}$	80
$\gamma_{32}$	25	$\gamma_{31}$	75
$\gamma_{76}$	20	$\gamma_{43}$	15
$\gamma_{53}$	45	$\gamma_{46}$	20
$\gamma_{56}$	20	$\gamma_{71}$	5
$\gamma_{72}$	10		

simulations [13] in different temporal regimes of laser excitation rate and find the stationary solution ( $\dot{\rho} = 0$ ). The ratio of remnant  $\text{NV}^-$  center is equal to  $\rho_{11} + \rho_{22} + \rho_{33} + \rho_{44} + \rho_{55}$ .

For the remnant NV centers, we also calculate their ODMR spectra with the above-mentioned method. Specifically, in the 3rd step, we only keep the remnant  $\text{NV}^-$ - $\text{N}^+$  pairs (with a ratio less than 1 as the laser excitation destroys partial of the  $\text{NV}^-$ - $\text{N}^+$  pairs). Figure S3 (b) shows the splitting and width of ODMR spectra as a function of the remnant  $\text{NV}^-$  ratio.

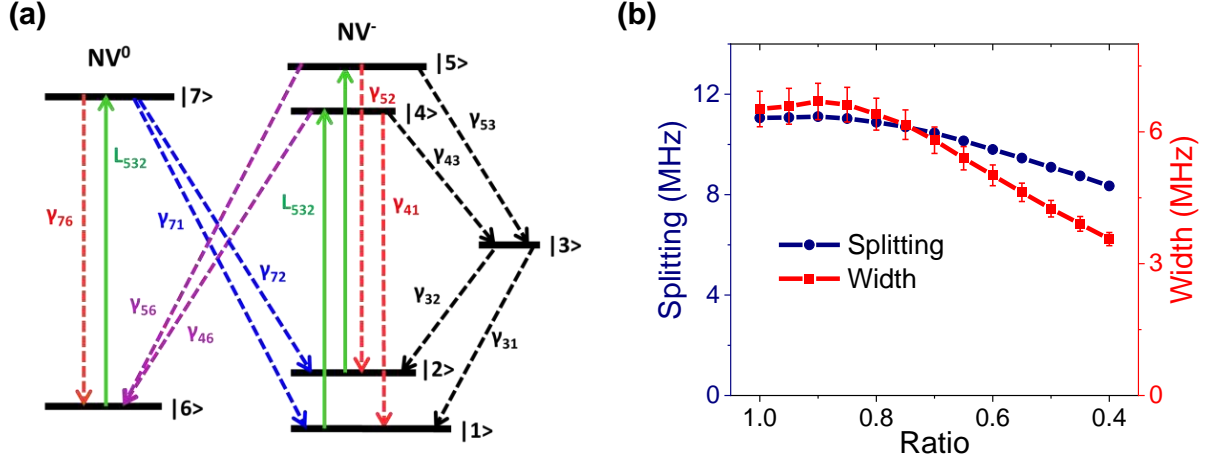


FIG. S3. (a) The model of photon-induced NV charge conversion. (b) For  $[N] = 100$  ppm,  $[NV] = 3$  ppm, the splitting and dependence on the remnant  $NV^-$  center ratios (the proportion of  $NV^-$ - $N^+$  pairs remaining under certain laser power).

#### IV. EXTENDED DATA: ODMR OF NANODIAMONDS AND MICRODIAMONDS

Figure S4 displays the ODMR spectra of four different nanodiamonds. In addition, ODMR spectra of four microdiamonds are shown in Fig. S5. The signals are normalized to the photon counts obtained when the MW frequency is far detuned. To estimate the splitting and width of these spectra, we use Eq. (20) in Sec. II to fit the ODMR data. The laser-induced narrowing and decreasing of splitting are observed for all the measured nanodiamonds and microdiamonds.



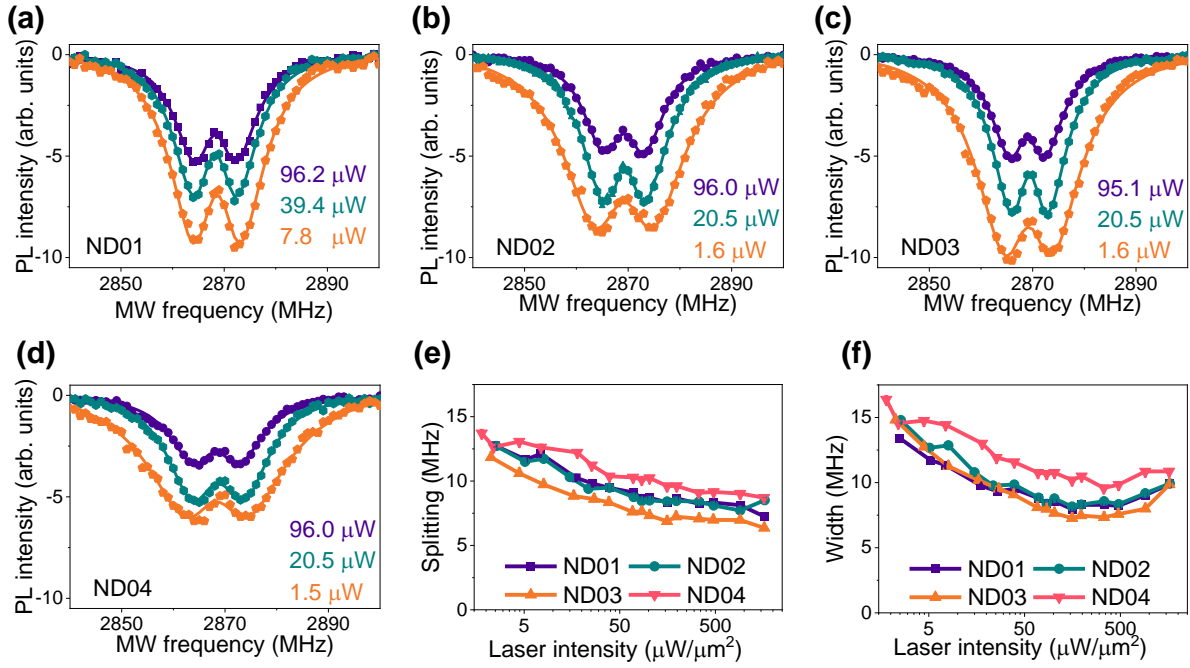


FIG. S4. The ODMR spectra of nanodiamonds under different laser powers. (a-d) are the typical ODMR data of four nanodiamond particles, respectively. (e) and (f) show the splitting and the width of ODMR spectra, respectively.

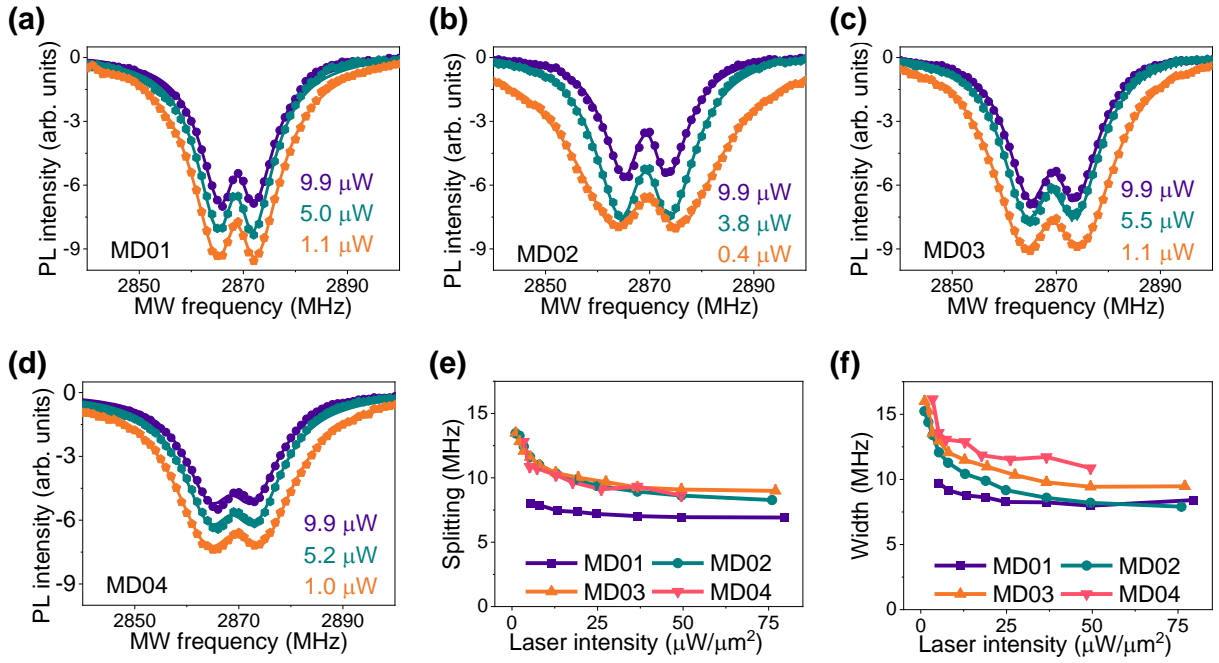


FIG. S5. The ODMR spectra of microdiamonds under different laser powers. (a-d) are the typical ODMR data of four microdiamond particles, respectively. (e) and (f) are the splitting and the width of ODMR spectra, respectively.

- 
- [1] N. B. Manson, M. Hedges, M. S. Barson, R. Ahlefeldt, M. W. Doherty, H. Abe, T. Ohshima, and M. J. Sellars, NV—N<sup>+</sup> pair centre in 1b diamond, *New J. Phys* **20**, 113037 (2018).
  - [2] T. Mittiga, S. Hsieh, C. Zu, B. Kobrin, F. Machado, P. Bhattacharyya, N. Rui, A. Jarmola, S. Choi, D. Budker, *et al.*, Imaging the local charge environment of nitrogen-vacancy centers in diamond, *Physical review letters* **121**, 246402 (2018).
  - [3] E. Van Oort and M. Glasbeek, Electric-field-induced modulation of spin echoes of nv centers in diamond, *Chemical Physics Letters* **168**, 529 (1990).
  - [4] S. Whitehead and W. Hackett, Measurement of the specific inductive capacity of diamonds by the method of mixtures, *Proceedings of the Physical Society (1926-1948)* **51**, 173 (1939).
  - [5] N. Aslam, G. Waldherr, P. Neumann, F. Jelezko, and J. Wrachtrup, Photo-induced ionization dynamics of the nitrogen vacancy defect in diamond investigated by single-shot charge state detection, *New Journal of Physics* **15**, 013064 (2013).
  - [6] X.-D. Chen, S. Li, A. Shen, Y. Dong, C.-H. Dong, G.-C. Guo, and F.-W. Sun, Near-infrared-enhanced charge-state conversion for low-power optical nanoscopy with nitrogen-vacancy centers in diamond, *Physical Review Applied* **7**, 014008 (2017).
  - [7] Z. Yuan, M. Fitzpatrick, L. V. Rodgers, S. Sangtawesin, S. Srinivasan, and N. P. De Leon, Charge state dynamics and optically detected electron spin resonance contrast of shallow nitrogen-vacancy centers in diamond, *Physical Review Research* **2**, 033263 (2020).
  - [8] P. Siyushev, H. Pinto, M. Vörös, A. Gali, F. Jelezko, and J. Wrachtrup, Optically controlled switching of the charge state of a single nitrogen-vacancy center in diamond at cryogenic temperatures, *Physical review letters* **110**, 167402 (2013).
  - [9] S. A. Savinov, V. V. Sychev, and D. Bi, Diamond nitrogen-vacancy center charge state ratio determination at a given sample point, *Journal of Luminescence* , 118981 (2022).
  - [10] R. P. Roberts, M. L. Juan, and G. Molina-Terriza, Spin-dependent charge state interconversion of nitrogen vacancy centers in nanodiamonds, *Physical Review B* **99**, 174307 (2019).
  - [11] R. Giri, C. Dorigoni, S. Tambalo, F. Gorrini, and A. Bifone, Selective measurement of charge dynamics in an ensemble of nitrogen-vacancy centers in nanodiamond and bulk diamond, *Physical Review B* **99**, 155426 (2019).
  - [12] G. Lindblad, On the generators of quantum dynamical semigroups, *Communications in Mathematical Physics* **48**, 119 (1976).
  - [13] S. M. Tan, A computational toolbox for quantum and atomic optics, *Journal of Optics B: Quantum and Semiclassical Optics* **1**, 424 (1999).